Boosting the Figure-Of-Merit of LSPR-Based Refractive Index Sensing by Phase-Sensitive Measurements

Kristof Lodewijks,*[†,‡] Willem Van Roy,[†] Gustaaf Borghs,[†,§] Liesbet Lagae,[†,§] and Pol Van Dorpe[†,‡]

[†]IMEC, Kapeldreef 75, B-3001 Leuven, Belgium

[‡]Department of Electrical Engineering (ESAT) and [§]Department of Physics and Astronomy, KU Leuven, Leuven, Belgium

S Supporting Information

ABSTRACT: Localized surface plasmon resonances possess very interesting properties for a wide variety of sensing applications. In many of the existing applications, only the intensity of the reflected or transmitted signals is taken into account, while the phase information is ignored. At the center frequency of a (localized) surface plasmon resonance, the electron cloud makes the transition between in- and out-of-phase oscillation with respect to the incident wave. Here we show that this information can experimentally be extracted by performing phase-sensitive measurements, which result in linewidths that are almost 1 order of magnitude smaller than those for intensity based measurements. As this phase change is an intrinsic property of a plasmon resonance, this opens up many possibilities for boosting the figure-of-merit (FOM) of refractive index sensing by taking into account the phase of the plasmon resonance. We experimentally investigated this for two model systems: randomly distributed gold nanodisks and gold nanorings on top of a continuous gold layer and a dielectric spacer and observed FOM values up to 8.3 and 16.5 for the respective nanoparticles.

KEYWORDS: LSPR sensing, refractive index sensing, plasmonics, spectroscopic ellipsometry, phase difference, retardation
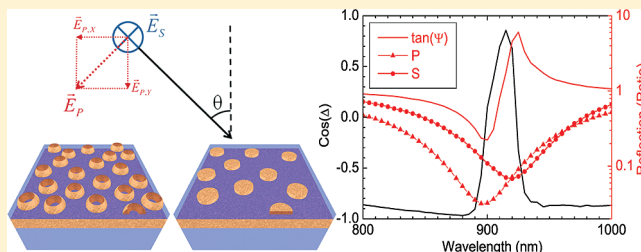
The collective oscillations of the free electrons in noble metals have been studied extensively over the past decades for a wide variety of applications. Both propagating surface plasmon polariton (SPP) and localized surface plasmon resonance (LSPR) modes possess very interesting properties with applications in sensing (refractive index sensing,[1−6] SERS[7]), metamaterials,[8] waveguiding[9,10] and enhanced coupling to active semiconductor components (e.g., photovoltaic cells,[11] SPASERs[12,13]). Refractive index sensing is by far the most studied application and allows label-free and real-time detection of changes in the dielectric environment of the plasmonic nanostructures. Moreover, by functionalizing the nanostructures, the sensors can be made specific to a particular molecule. In former works, research groups have followed various paths in order to optimize the nanostructure designs such that higher sensitivities, figures-of-merit (FOM), and lower detection limits (DLs) can be achieved. Plasmon resonances are extremely sensitive to the refractive index of the surrounding medium. With increasing values of the refractive index the LSPR shows a red shift, and the magnitude of this shift divided by the change in refractive index is defined as the sensitivity ($d\lambda/dn$). The figure-of-merit of a plasmon resonance is given by the ratio between the sensitivity and the width of the resonance peak (FOM = $(d\lambda/dn)/$fwhm), and high values of the FOM are an indication for good sensor performance. For structures with increased FOMs, the DLs (smallest refractive index change which can be measured) can be reduced. Recently a lot of progress has been made in line width tuning (Fano resonances, subradiance) in order to obtain higher FOMs.[1,2,14−18]

In any resonant system, a pronounced transition from in- to out-of-phase oscillation is observed around the center frequency of the resonance with respect to the driving force. This is also the case for (localized) surface plasmon resonances, where the electron cloud makes the transition between in- and out-of-phase oscillation with respect to the incident wave.[18] Also for conventional SPR sensing, it was shown that these phase changes can be probed by phase sensitive measurements, which show a much smaller spectral/angular footprint compared to their intensity based counterparts.[3,4] Here we show that using standard spectroscopic ellipsometry measurements, we can measure similar phase jumps around the center frequency of localized surface plasmon resonances. For our two model systems, we investigated the angle- and polarization-dependent reflection spectra and the phase difference between P- and S-polarized waves, using lock-in measurements.

In this work, we investigated localized surface plasmon resonances in randomly distributed gold nanoparticles on top of a continuous gold layer and a dielectric spacer by spectroscopic ellipsometry. The investigated sample structures are illustrated in Figure 1 and consist of a glass substrate covered with a 100 nm gold (Au) layer, a 50 nm silica (SiO₂)
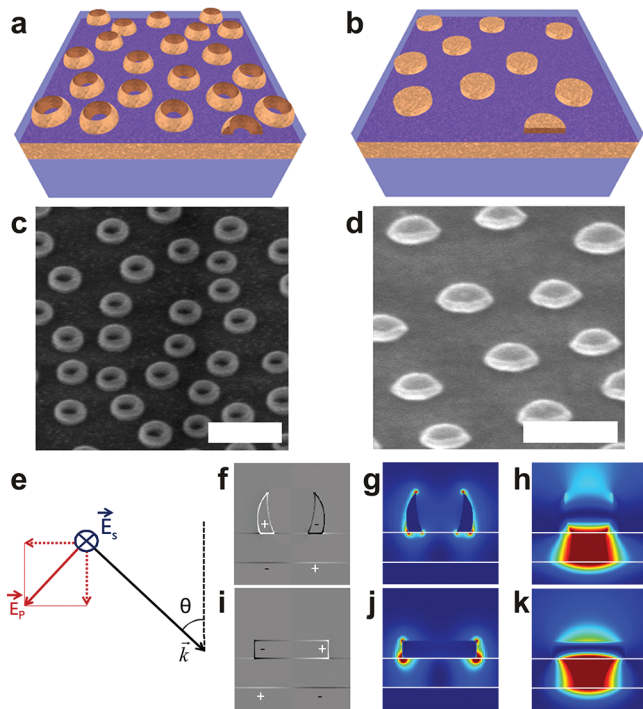
Figure 1. Overview of the sample structure, measurement configuration and the involved plasmonic modes. (a,b) Schematic sample overview of a 1 μm^2 area of rings and disks. (c,d) Scanning electron microscope pictures of the ring and disk samples. Scale bar 500 nm. (e) Measurement configuration for the two polarization states. (f,i) Simulated charge plots at resonance for rings and disks. (g,j) Simulated electric field intensity at the electric dipole resonance for rings and disks. (h,k) Simulated induced magnetic dipole for rings and disks.

spacer and randomly distributed Au nanoparticles that were fabricated using colloidal lithography.[19,20] The nanorings (Figure 1a,c) have an outer diameter of 150 nm and a height of 60 nm while the less densely packed nanodisks (Figure 1b,d) have a diameter of 140 nm and a height of 30 nm. The average (center-to-center) interparticle distance is 250 nm for nanorings and 350 nm for nanodisks.

By scanning the angle of incidence, the electric dipole resonances (Figure 1g,j) in the nanoparticles become spectrally detuned for both polarization states. Both for P- and S-polarized waves, the electric dipole in the nanoparticle couples to an electric quadrupole in the combined nanoparticle/gold film complex (Figure 1f,i), which gives rise to an induced magnetic dipole (Figure 1h,k) perpendicular to the electric dipole in the nanoparticle.

The angle dependent spectroscopic ellipsometry measurements were performed using a commercial GESP5[21] ellipsometer and a home-built setup based on a photoelastic modulator (PEM).[22] For the GESP5 setup, the polarization of the incident beam is modulated between P and S by a rotating polarizer, while for the PEM-based setup, the polarization is modulated between linear and left- and right-circular polarization states. Both measurement setups have different signal-to-noise ratios in different spectral ranges, so depending on the spectral position of the LSPR we choose the setup that performs best. All spectroscopic ellipsometry measurements shown here were performed with the GESP5 setup, except for the refractive index sensing measurements on gold rings in Figure 5b.

The phase information is extracted by performing lock-in measurements at the modulation frequency. The measured quantities $\tan(\Psi)$ and $\cos(\Delta)$ are related by the main equation of ellipsometry

$$\rho = \frac{R_P}{R_S} = \tan(\Psi)\exp(i\Delta)$$

$$= \tan(\Psi)(\cos(\Delta) + i\sin(\Delta)) \qquad (1)$$

and represent the amplitude reflection ratio between P and S ($\tan(\Psi)$) and the phase difference between the reflected signals Δ for the 2 polarizations (reflected in the $\cos(\Delta)$ value).

In that way, the angle dependence of the plasmon resonances and the extremely narrow phase changes at their central frequency could be probed experimentally. By properly designing the nanoparticle shape and density, the interparticle coupling can be tuned resulting in two spectrally slightly detuned resonances for P- and S-polarized incident light. An overview of the angle dependent measurements on the nanorings is given in Figure 2. Panels a and b show the
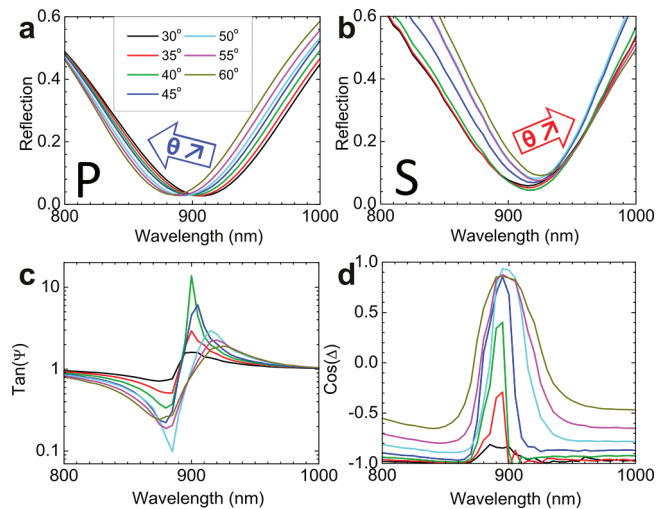

Figure 2. Angle dependent measurement data for gold nanorings. (a,b) Measured intensity based reflection spectra for P- and S-polarizations. (c) Measured values of $\tan(\Psi)$, the amplitude reflection ratio between P- and S-polarizations. (d) Measured values of $\cos(\Delta)$, with Δ the phase difference between both polarization states.

intensity based reflection spectra for P- and S-polarized incident waves, while panels c and d show the reflection ratio $\tan(\Psi)$ and the phase difference $\cos(\Delta)$ between the two polarization states. With increasing incident angle, the P-resonance shows a blue shift, while the S-resonance shows a red shift. These resonance shifts are reflected in the phase sensitive ellipsometry measurements in which at the center frequency of the plasmon resonances a minimum and maximum in the reflection ratio (Figure 2c), and a pronounced phase difference between P and S (Figure 2d) is observed.

The angle- and polarization dependent optical response of our samples was simulated using Comsol multiphysics[23] (Figure 3). The different spectra were calculated for a square lattice of rings with a pitch of 250 nm (matched to the experimental average interparticle distance). By using periodic (Bloch) boundary conditions and scanning all the angles involved for both polarizations, the angle dependent reflection and the ellipsometric parameters were extracted. The reflected
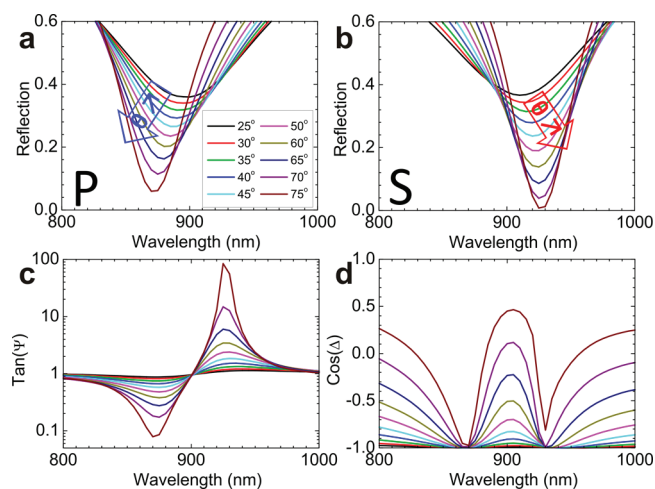
Figure 3. Angle-dependent simulation data for a periodic array of gold nanorings. (a,b) Simulated intensity based reflection spectra for P- and S-polarizations. (c) Simulated values of tan(Ψ), the reflection ratio between P- and S-polarizations. (d) Simulated values of cos(Δ) with Δ the phase difference between both polarization states.

Figure 4. Angle-dependent measurements on gold nanodisks. Reflection spectra for P- (a) and S-polarization (b). (c) Reflection ratio tan(Ψ). (d) Phase difference cos(Δ).

waves for P- and S-polarized waves were recorded and their electric and magnetic fields were averaged out over one unit cell, allowing to extract the amplitude and phase in order to evaluate the values of tan(Ψ) and cos(Δ). We used a periodic particle arrangement in order to take into account the interactions between the neighboring particles, as these determine the spectral shifts of the modes for P and S with changing angles of incidence. Simulations on single particles would not include these interactions, and finite element simulations on a random particle distribution were not possible due to computational limitations. A nice qualitative agreement is obtained, where the P-resonance and S-resonances show the blue shift (Figure 3a) and red shift (Figure 3b), respectively, similar to the experimental data. Contrary to the measured data, the minimum of the reflection dip shows a decrease with increasing angle of incidence. This behavior can be attributed to the random particle distribution in our samples, that gives rise to inhomogeneous broadening, which is most pronounced for large angles of incidence due to increasing spot sizes. This explains why the maxima and minima in the reflection ratio (tan(Ψ)) are not observed at the largest angle of incidence in the experimental spectra, contrary to the simulated data (Figure 3c). Interestingly, if we compare the magnitude of the phase difference between P and S, we clearly observe that the largest phase changes are observed at the maxima and minima in the reflection ratio, which occur around 45° in the experiments (Figure 2d), and at 75° in simulations (Figure 3d).

Similar measurements were performed for gold nanodisks, which have comparable sizes to the rings, but are less densely packed due to different fabrication parameters. An overview of the angle dependent measurements for both polarizations is given in Figure 4. Both for P- (Figure 4a) and S-polarized (Figure 4b) waves, the electric dipole resonances are blue-shifted compared to the nanorings. With increasing angle of incidence, for the P-polarization, a minor blue shift is observed, while the S-resonance shows a pronounced red shift. Both resonances show much more spectral overlap compared to the nanorings, which results in a totally different behavior in their reflection ratio tan (Ψ) (Figure 4c). For small angles of incidence we observe a maximum in the reflection ratio at
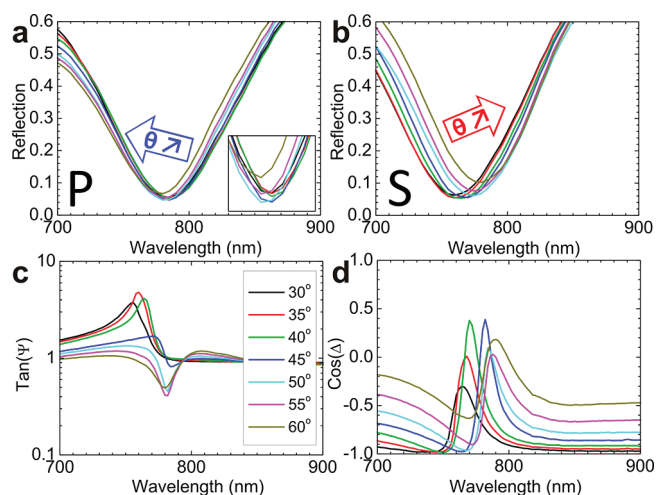
shorter wavelengths, while at larger angles of incidence the S-resonance shifts to longer wavelengths with respect to the P-resonance, resulting in similar spectra as for gold nanorings. If we take a closer look at the phase difference between P and S (Figure 4d), we observe again two phase jumps, one for each polarization state, which are smaller in magnitude compared to the nanorings. These smaller phase jumps can be attributed to the increased spectral overlap for the two polarization states, which results in a smaller overall phase difference.

For the two nanoparticle geometries, we have illustrated that we can clearly identify the phase changes at the LSPR frequency for the different polarization states. Now we want to take a closer look at the plasmon modes involved and the dominating interparticle coupling mechanism. For both polarization states an electric dipole is excited in the nanoparticle (Figure 1g,j), which shows a very broad line width (around 140 nm for rings and 100 nm for disks). This electric dipole resonance couples directly (P-polarization) or capacitively (S-polarization) to an electric quadrupole mode in the combined nanoparticle/gold film complex (Figure 1f,i). The electric quadrupole mode also results in an induced magnetic dipole moment (Figure 1h,k), which is aligned perpendicular to the electric dipole in the nanoparticles. By varying the angle of incidence and the polarization, the phase retardation is scanned, resulting in different coupling efficiencies to the plasmon modes and differences in the interparticle coupling strength, which is reflected in spectral shifts of the plasmon resonances.[24] The interparticle coupling is mediated by electric dipole/quadrupole coupling and magnetic dipole coupling, both in the longitudinal and transversal direction. If the scattered fields of the nanoparticle are in phase (out of phase) with the incident wave in the neighboring particles, the local resonance will be enhanced (opposed) and show a blue (red) shift. We investigated the interparticle coupling by numerical simulations on 1D linear arrays of the respective nanoparticles and were able to identify the dominating interparticle coupling mechanisms for the different polarization states (see Supporting Information). For P-polarized excitation, the coupling is dominated by longitudinal magnetic coupling and transverse electric coupling, while for the S-polarized excitation the coupling is dominated by longitudinal electric coupling and transverse magnetic coupling.

In a next step, the samples were mounted in a flowcell to perform bulk refractive index sensing measurements with different concentrations of glycerol in water. An overview of these measurements is presented in Figure 5. In panel a, the
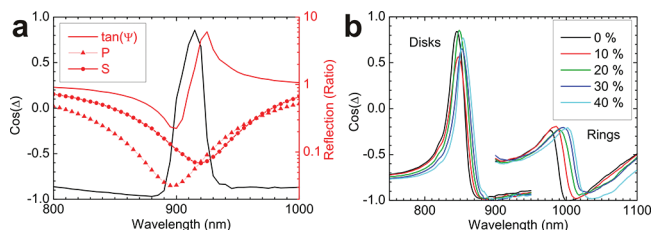

Figure 5. Refractive index sensing measurements on gold nanodisks and nanorings for 45° incidence. (a) Comparison of phase-sensitive measurements (black) and intensity based measurements (red) on gold nanorings in air, illustrating a dramatic line width reduction in the phase-difference between P and S. (b) Refractive index sensing measurements on disks and disks with variable concentrations of glycerol in water.

line width reduction for the phase-sensitive measurements with respect to the intensity-based reflection measurements is clearly illustrated for nanorings in air. At the dip of the LSPR for both polarization states, a narrow phase change is observed in $\cos(\Delta)$. Panel b shows the wavelength shift as function of increasing glycerol concentrations in water. Here we used an incident angle of 70°, such that the incident angle at the sample/solution interface matches the 45° incident angle of the reference measurement in air. As expected, with increasing refractive index, we observe a red shift of the resonance positions for both polarization states. Different plasmon modes are excited for P- and S-polarization, which show different sensitivities to the refractive index. Moreover, depending on the spectral position of both resonances and their spectral overlap, the shape of the $\cos(\Delta)$ signals can change dramatically for the different nanoparticles. This effect is clearly observed when comparing the spectra for disks and rings in air and in solution. If the plasmon modes for P and S show a lot of spectral overlap, the maximum phase difference between the 2 modes will be reduced significantly. We clearly observe this reduction for the rings the sensing solution (Figure 5b) and the disks in air (Figure 4), where the overlap of the modes is the largest. This implies that for the gold rings the sensitivity of the P-mode is much larger than for the S-mode, as they are separated by about 30 nm in air, while in the sensing solutions they clearly show spectral overlap. In order to calculate the figure of merit of the two model systems, we calculated the sensitivities for the combined phase-sensitive $\cos(\Delta)$ signals of the P- and S-modes and compared these with the amplitude based reflection data. In the overview presented in Table 1, we can clearly see that the phase sensitive measurements show much narrower line widths compared to their intensity-based counterparts. Because of this dramatic decrease in the spectral footprint, the FOM could be boosted 3.9 and 6.1 times up to 8.3 and 16.5 for nanodisks and nanorings respectively. For the samples presented here, we did not optimize the structures in order to reach the smallest possible line widths. This implies that there is still a lot of room for improvement in the sample design. The effects of inhomogeneous broadening can be largely suppressed by studying periodic arrays. Moreover, by looking at asymmetric particles the resonances for P and S can be spectrally detuned and in that way one could easily fit the linewiths of a single

Table 1. Comparison between Intensity- and Phase-Sensitive Reflection Measurements on Gold Nanodisks and Nanorings at an Incidence Angle of 45°

	disks	rings
$d\lambda/dn$ (nm/RIU)	208.0	380.0
fwhm reflection (nm)	98.0	139.0
FOM reflection	2.1	2.7
fwhm $\cos(\Delta)$ (nm)	25.0	23.0
FOM $\cos(\Delta)$	8.3	16.5
FOM increase ratio	3.9	6.1

resonance instead of the combined line width as we did in this work. Here we mainly focused on proof-of-principle and therefore we restricted our measurements to bulk changes in the refractive index. For structures similar to the ones described here, we expect the decay length for the field enhancements to be several tens of nanometers,[5] which implies that these samples could also be applied for biological sensing using antibody/antigen interactions, where the improved FOM could result in lower detection limits.

To summarize, we have shown that the FOM for reflection based refractive index sensing can be largely increased by measuring the phase of the reflected beam instead of its intensity only. Around the center frequency of the LSPR, the electron cloud makes the transition of in- to out-of-phase oscillation with respect to the driving field, which is an intrinsic property of a plasmon resonance. This phase difference shows a much smaller spectral footprint than the intensity-based reflection measurements, resulting in much narrower line widths and largely increased values of the FOM. For the nanoparticles investigated in this work, we managed to increase the FOM up to 6 times for intrinsically broad dipole resonances.

■ ASSOCIATED CONTENT

Ⓢ Supporting Information
Additional simulations on 1D periodic arrays of the respective nanostructures showing the dominant interparticle coupling mechanisms. This material is available free of charge via the Internet at http://pubs.acs.org.

■ AUTHOR INFORMATION

Corresponding Author
*E-mail: kristof.lodewijks@imec.be.

■ ACKNOWLEDGMENTS

■ REFERENCES

(1) Hao, F.; Nordlander, P.; Sonnefraud, Y.; Van Dorpe, P.; Maier, S. A. Tunability of Subradiant Dipolar and Fano-Type Plasmon Resonances in Metallic Ring/Disk Cavities: Implications for Nanoscale Optical Sensing. *ACS Nano* **2009**, *3*, 643−652.

(2) Verellen, N.; Van Dorpe, P.; Huang, C.; Lodewijks, K.; Vandenbosch, G. A. E.; Lagae, L.; Moshchalkov, V. V. Plasmon Line Shaping using Nanocrosses for High sensitivity LSPR Sensing. *Nano Lett.* **2011**, *11* (2), 391−397.

(3) Kabashin, A. V.; Nikitin, P. I. Surface plasmon resonance interferometer for bio- and chemical-sensors. *Opt. Commun.* **1998**, *150*, 5−8.

(4) Kabashin, A. V.; Patskovsky, S.; Grigorenko, A. N. Phase and amplitude sensitivities in surface plasmon resonance bio and chemical sensing. *Opt. Expr.* **2009**, *17*, 21191−21204.

(5) Chen, S.; Svedendahl, M.; Kll, M.; Gunnarsson, L.; Dmitriev, A. Ultrahigh sensitivity made simple: nanoplasmonic label-free biosensing with an extremely low limit-of-detection for bacterial and cancer diagnostics. *Nanotechn.* **2009**, *20*, 434015.

(6) Anker, J. N.; Paige Hall, W.; Lyandres, O.; Shah, N. C.; Zhao, J.; Van Duyne, R. P. Biosensing with plasmonic nanosensors. *Nat. Mater.* **2008**, *7*, 442−453.

(7) Ye, J.; Shioi, M.; Lodewijks, K.; Lagae, L.; Kawamura, T.; Van Dorpe, P. Tuning plasmonic interaction between gold nanorings and a gold film for enhanced Raman Scattering. *Appl. Phys. Lett.* **2010**, *97*, 163106.

(8) Lodewijks, K.; Verellen, N.; Van Roy, W.; Borghs, G.; Van Dorpe, P. Self-assembled hexagonal double fishnets as negative index materials. *Appl. Phys. Lett.* **2011**, *98*, 091101.

(9) Neutens, P.; Van Dorpe, P.; De Vlaminck, I.; Lagae, L.; Borghs, G. Electrical detection of surface plasmon polaritons in metallic slot waveguides. *Nat. Photon.* **2009**, *3*, 283−286.

(10) Neutens, P.; Van Dorpe, P.; Lagae, L.; Borghs, G. Electrical excitation of confined surface plasmon polaritons in metallic slot waveguides. *Nano Lett.* **2010**, *10*, 1429−1432.

(11) Atwater, H.; Polman, A. Plasmonics for improved photovoltaic devices. *Nat. Mater.* **2010**, *9*, 205−213.

(12) Zheludev, N. I.; Prosvirnin, S. L.; Papasimakis, N.; Fedotov, V. A. Lasing spaser. *Nat. Photon.* **2008**, *6*, 351−354.

(13) Noginov, M. A.; Zhu, G.; Belgrave, A. M.; Bakker, R.; Shalaev, V. M.; Narimanov, E. E.; Stout, S.; Herz, E.; Suteewong, T.; Wiesner, U. Demonstration of a spaser-based nanolaser. *Nature* **2009**, *460*, 1110−1112.

(14) Evlyukhin, A. B.; Bozhevolnyi, S. I.; Pors, A.; Nielsen, M. G.; Radko, I. P.; Willatzen, M.; Albrektsen, O. Detuned Electrical Dipoles for Plasmonic sensing. *Nano Lett.* **2010**, *10*, 4571−4577.

(15) Hao, F.; Sonnefraud, Y.; Van Dorpe, P.; Maier, S. A.; Halas, N. J.; Nordlander, P. Symmetry Breaking in Plasmonic Nanocavities: Subradiant LSPR Sensing and a Tunable Fano Resonance. *Nano Lett.* **2008**, *8*, 3983−3988.

(16) Luk'yanchuk, B.; Zheludev, N. I.; Maier, S. A.; Halas, N. J.; Norlander, P; Giessen, H; Chong, T. C. The Fano resonance in plasmonic nanostructures and metamaterials. *Nat. Mater.* **2010**, *9*, 707−715.

(17) Offermans, P.; Schaafsma, M. C.; Rodriguez, S. R. K.; Zhang, Y.; Crego-Calama, M.; Brongersma, S. H.; Gomez Rivas, J. Universal Scaling of the Figure of Merit of Plasmonic Sensors. *ACS Nano* **2011**, *5*, 5151−5157.

(18) Kravets, V. G.; Schedin, F.; Kabashin, A. V.; Grigorenko, A. N. Sensitivity of Collective Plasmon Modes of Gold Nanoresonators to Local Environment. *Opt. Lett.* **2010**, *35*, 956−958.

(19) Ye, J.; Van Dorpe, P.; Lagae, L.; Maes, G.; Borghs, G. Observation of plasmonic dipolar anti-bonding mode in silver nanoring structures. *Nanotechnology* **2010**, *20*, 465203.

(20) Frederikson, H.; Alaverdyan, Y.; Dmitriev, A.; Langhammer, C.; Sutherland, D. S.; Zach, M.; Kasemo, B. Hole-Mask Colloidal Lithography. *Adv. Mater.* **2007**, *19*, 4297−4302.

(21) GESP 5 ellipsometer, SOPRALAB, 55, avenue de l'Europe, 92400 COURBEVOIE, France

(22) Jasperson, S. N.; Schnatterly, S. E. An Improved Method for High Refl ectivity Ellipsometry Based on a New Polarization Modulation Technique. *Rev. Sci. Instrum.* **1969**, *40*, 761.

(23) Comsol Multiphysics 3.5a (RF Module), 1 New England Executive Park, Suite 350, Burlington, MA 01803, USA

(24) Pinchuk, A. O. Angle Dependent Collective Surface Plasmon Resonance in an Array of Silver Nanoparticles. *J. Phys. Chem. A* **2009**, *113*, 4430.